

# Renormalization of Bilinear Quark Operators for Overlap Fermions

Thomas DeGrand and Zhaofeng Liu

*Department of Physics, University of Colorado, Boulder, CO 80309 USA*

We present non-perturbative renormalization constants of fermionic bilinears on the lattice in the quenched approximation at  $\beta = 6.1$  using an overlap [1] fermion action with hypercubic(HYP)-blocked links. We consider the effects of the exact zero modes of the Dirac operator and find they are important in calculating the renormalization constants of the scalar and pseudoscalar density. The results are given in the RI' and  $\overline{MS}$  schemes and compared to the perturbative calculations.

## I. INTRODUCTION

This paper describes the computation of matching factors for converting lattice calculations of matrix elements of currents to the corresponding values measured in a continuum  $\overline{MS}$  scheme. The lattice action uses overlap fermions [1] and HYP-blocked links [2].

We use the nonperturbative methodology introduced in Ref. [3]. The proposed renormalization scheme is one which can be implemented not only in lattice Monte Carlo simulation but also in continuum perturbation theory. Thus, the conversion of lattice results to a more conventional scheme such as  $\overline{MS}$  is possible. In this scheme, the matrix element of a bilinear quark operator  $O_\Gamma = \bar{\psi}\Gamma\psi$  between quark fields at certain momentum  $p^2 = \mu^2$  is computed and matched to the corresponding tree level matrix element. i.e. the renormalization condition is

$$Z_\Gamma \langle p|O_\Gamma|p \rangle_{p^2=\mu^2} = \langle p|O_\Gamma|p \rangle_{tree}. \quad (1)$$

Here  $\Gamma$  can be any combination of Dirac matrices. This method is supposed to work when  $\mu$  satisfies

$$\Lambda_{QCD} \ll \mu \ll 1/a. \quad (2)$$

The discretization effects are under control if the renormalization scale  $\mu$  is much smaller than the lattice cut off  $1/a$ .  $\Lambda_{QCD} \ll \mu$  guarantees that the non-perturbative effects are ignorable.

There have been many calculations using this scheme. Ref. [3] used improved Wilson fermions, Ref. [4] used both the Wilson and the tree level improved SW-Clover fermion action in the quenched approximation, Ref. [5] worked with standard Wilson fermions ( $r = 1$ ) in the quenched approximation, Ref. [6] used chirally improved lattice fermions in the quenched approximation. Here, we use overlap fermions [1] in the quenched approximation. Specifically, we work with overlap fermions built from a "kernel action" with nearest and next-nearest neighbor fermionic interactions [7] and hypercubic(HYP)-blocked links [2]. Overlap fermions respect chiral symmetry on the lattice via the Ginsparg-Wilson relation [8], while for Wilson-type fermions, the Wilson term breaks the chiral symmetry explicitly. Chirally improved fermions only obey the Ginsparg-Wilson relation approximately.

Lattice perturbation theory is probably the most often used way to calculate the renormalization factors. However, the convergence of the perturbative series is often not satisfying. To improve the convergence of the series, Lepage and Mackenzie proposed a tadpole improved perturbation theory [9]. Nevertheless, lattice perturbation series rarely extend beyond the one-loop level, which is an important source of uncertainty in the extraction of physical results.

One-loop perturbative calculations of the matching coefficients between matrix elements measured in lattice simulations and their equivalent  $\overline{MS}$  values for the same overlap fermions and HYP-blocked links that we use here were done in Ref. [10]. Those perturbative results turned out to be quite close to unity, and they were used in computing the Kaon B parameter [11]. This work will give a non-perturbative check of the matching coefficients.

Perturbative results of the matching coefficients for other actions also using HYP-blocked links or similar gauge connections were presented in [12]. They show the same behavior that the matching coefficients are quite close to unity. Our results may be useful to others doing simulations with HYP links, to give an idea how trustworthy perturbation theory is.

In Eq. (1),  $\Gamma$  can be any combination of Dirac matrices. We will consider the cases  $\Gamma = I, \gamma_5, \gamma_\mu$  and  $\gamma_\mu\gamma_5$ , which we will denote S, P, V and A respectively. Chiral symmetry implies several relations between renormalization constants for overlap fermions, in particular  $Z_S = Z_P$  and  $Z_V = Z_A$ .

The paper is organized as follows: In Section II, we briefly discuss the non-perturbative renormalization method [3], the overlap action and how we deal with the zero modes of the Dirac operator. Numerical results are given in Section III. The formulas for conversion to  $\overline{MS}$  scheme are recapitulated in Section IV. We will compare our results with perturbative calculations in Section V and conclude in Section VI.

## II. METHODOLOGY

The following is a brief summary of the method from Ref. [3, 6], a short description of the overlap action we used (for a detail description, see Ref. [7]) and how we deal with the zero modes of the Dirac operator. For convenience, the lattice spacing  $a$  is set to be one.

From Eq. (1), we have

$$Z_\Gamma \frac{1}{12} \text{Tr} \left[ \langle p | O_\Gamma | p \rangle \langle p | O_\Gamma | p \rangle_{tree}^{-1} \right] \Big|_{p^2=\mu^2} = 1. \quad (3)$$

Here  $\frac{1}{12}$  comes from the fact that the trace is over color and spin space. Since

$$\langle p | O_\Gamma | p \rangle = Z_q \Lambda_\Gamma(p), \quad (4)$$

we obtain

$$Z_\Gamma = \frac{12}{Z_q \text{Tr} \left[ \Lambda_\Gamma(p) \langle p | O_\Gamma | p \rangle_{tree}^{-1} \right]} \Big|_{p^2=\mu^2}. \quad (5)$$

Here  $Z_q$  is the quark field renormalization constant (The bare field  $\psi_0 = Z_q^{1/2} \psi$ ) and  $\Lambda_\Gamma(p)$  is the amputated Green function

$$\Lambda_\Gamma(p) = S^{-1}(p) G_\Gamma(p) S^{-1}(p), \quad (6)$$

where  $S(p)$  is the quark propagator. Eq. (5) is the formula we will use to calculate  $Z_\Gamma$ .

$Z_q$  is obtained by comparing the quark propagator to the free lattice propagator (the RI' scheme):

$$Z_q^{RI'} = \frac{1}{12} \text{Tr} [S(p) D_f^{ov}(p)] \Big|_{p^2=\mu^2}, \quad (7)$$

where  $D_f^{ov}(p)$  is the free lattice overlap Dirac operator. (Our  $Z_q$  is the inverse of the quark field renormalization constant in Ref. [6].)

The Green function  $G_\Gamma(p)$  is determined in the following way.

$$\begin{aligned} G_\Gamma(p) &= \sum_{x,y} e^{-ip \cdot (x-y)} \langle \psi(x) O_\Gamma(0) \bar{\psi}(y) \rangle \\ &= \sum_{x,y} e^{-ip \cdot (x-y)} \frac{1}{N} \sum_{i=1}^N S_i(x|0) \Gamma S_i(0|y) \\ &= \frac{1}{N} \sum_{i=1}^N \left( \sum_x S_i(x|0) e^{-ip \cdot x} \right) \Gamma \left( \sum_y S_i(0|y) e^{ip \cdot y} \right), \end{aligned} \quad (8)$$

where  $N$  is the number of gauge configurations. Using  $S_i(x|y) = \gamma_5 S_i(y|x)^\dagger \gamma_5$  and  $S_i(p|0) = \sum_x S_i(x|0) e^{-ip \cdot x}$ , we have

$$G_\Gamma(p) = \frac{1}{N} \sum_{i=1}^N S_i(p|0) \Gamma \gamma_5 S_i^\dagger(p|0) \gamma_5. \quad (9)$$

The quark propagator in momentum space is given by

$$S(p) = \frac{1}{N} \sum_{i=1}^N S_i(p|0). \quad (10)$$

$S_i(x|0)$  is computed on the lattice with a point source

$$\sum_x D^{ov}(z, x) S_i(x|0) = \delta_{z,0}. \quad (11)$$

(In Ref. [5] and Ref. [6], momentum sources were used.) At tree level,  $\langle p|O_\Gamma|p\rangle_{tree} = \Gamma$ . Therefore, every quantity on the right hand side of Eq. (5) is known and then we can obtain  $Z_\Gamma$ . For  $\Gamma = \gamma_\mu, \gamma_\mu\gamma_5$ , the index  $\mu$  is averaged under the trace in Eq. (5).

We fix the gauge to Landau gauge. Uncertainty due to Gribov copies is not investigated here. It has been discussed in Ref. [6, 13, 14, 15]. The effect was found to be negligible in current lattice simulations.

The overlap action that we use is described with detail in Ref. [7], which uses a "kernel" action with nearest and next-nearest neighbor couplings. The massless overlap Dirac operator is

$$D(0) = x_0 \left( 1 + \frac{z}{\sqrt{z^\dagger z}} \right), \quad (12)$$

where  $z = d(-x_0)/x_0 = (d - x_0)/x_0$  and  $d(m) = d + m$  is the massive Dirac operator for mass  $m$ . The overall multiplicative factor of  $x_0$  is a useful convention so that when  $D(0)$  is expanded for small  $d$ ,  $D \approx d$ .

The massive overlap Dirac operator is defined as

$$D(m) = \left( 1 - \frac{m}{2x_0} \right) D(0) + m. \quad (13)$$

In a background gauge field carrying a topological charge  $Q$ ,  $D(0)$  will have  $|Q|$  pairs of real eigenmodes with eigenvalues 0 and  $2x_0$ . In computing propagators, it is convenient to clip out the eigenmode with real eigenvalue  $2x_0$ , and to define the subtracted propagator as

$$\tilde{D}(m)^{-1} = \frac{1}{1 - \frac{m}{2x_0}} \left[ D(m)^{-1} - \frac{1}{2x_0} \right]. \quad (14)$$

This also converts local currents into order  $a^2$  improved operators [16]. Then the free lattice overlap Dirac operator  $D_f^{ov}(p)$  used in Eq. (7) is just  $\tilde{D}(m)$  in the momentum space.

The HYP-blocked links are constructed in three steps [2]. The parameters  $\alpha_1$ ,  $\alpha_2$  and  $\alpha_3$  in our simulation have the favored values of Ref. [2]: 0.75, 0.6 and 0.3 respectively.

A finite volume artifact we encounter in this quenched simulation is the presence of exact zero modes of the Dirac operator. The zero mode contribution (with positive chirality) in the propagator  $S_i(p|0)$  on a configuration with  $Q \neq 0$  takes the form

$$\frac{1}{m} \begin{pmatrix} |\phi_0(p)\rangle\langle\phi_0(p)| & 0 \\ 0 & 0 \end{pmatrix} \equiv \frac{1}{m} S_0 \quad (15)$$

in  $\gamma_5$  diagonal basis. Here  $|\phi_0(p)\rangle$  is the Fourier transform of the zero mode wave function  $|\phi_0(x)\rangle$ . Since the zero modes are localized in space,  $|\phi_0(p)\rangle$  will peak at low  $p$ . These zero modes do not resemble free field modes. Implicit in the RI' scheme analysis is the idea that at big  $\mu$ , lattice propagators resemble continuum ones. Zero modes clearly do not. In Section III, we will find zero modes make a large contribution to  $Z_S$  and  $Z_P$ . We believe this is because our lattice is not large.

The following little parametrization illustrates our expectations of the effects of zero modes:  $S_i(p|0)$  is the sum of the zero mode contribution and the non-zero mode contribution  $S_n$ ,

$$S_i(p|0) = \frac{1}{m} S_0 + S_n. \quad (16)$$

Therefore in Eq. (9)

$$S_i(p|0)\Gamma\gamma_5 S_i^\dagger(p|0)\gamma_5 = \frac{1}{m^2} S_0\Gamma\gamma_5 S_0^\dagger\gamma_5 + \frac{1}{m} (S_0\Gamma\gamma_5 S_n^\dagger\gamma_5 + S_n\Gamma\gamma_5 S_0^\dagger\gamma_5) + S_n\Gamma\gamma_5 S_n^\dagger\gamma_5, \quad (17)$$

and then  $G_\Gamma(p)$  can be written in the form

$$G_\Gamma(p) = \frac{1}{m^2} G_2 + \frac{1}{m} G_1 + G_0, \quad (18)$$

where the subscript counts the number of zero modes:  $G_0$  contains no zero mode contribution. The quark propagator averaged over all configurations and its inverse, if expanded for small  $m$ , are

$$\begin{aligned} S(p) &= \frac{1}{m} \bar{S}_0 + \bar{S}_n, \\ S^{-1}(p) &= m\bar{S}_0^{-1} - m^2\bar{S}_0^{-1}\bar{S}_n\bar{S}_0^{-1} + \dots \end{aligned} \quad (19)$$

Thus the amputated Green function

$$\begin{aligned}
\Lambda_\Gamma(p) &= S^{-1}(p)G_\Gamma(p)S^{-1}(p) \\
&= \left(\frac{1}{m}\bar{S}_0 + \bar{S}_n\right)^{-1} \left(\frac{1}{m^2}G_2 + \frac{1}{m}G_1 + G_0\right) \left(\frac{1}{m}\bar{S}_0 + \bar{S}_n\right)^{-1} \\
&\rightarrow \bar{S}_0^{-1}G_2\bar{S}_0^{-1} \quad \text{when } m \text{ is small.}
\end{aligned} \tag{20}$$

So, if the zero modes affect our calculation of  $Z_\Gamma$  (Eq. (5)), the effect should be evident at small momentum and small quark mass. Unfortunately, for us,  $\mu = 2$  GeV, where we will match, is rather small momentum.

We examine two solutions to those zero modes. One solution is to explicitly subtract the contribution of the zero modes in the quark propagator. We would prefer not to do this. The other solution is to use combination of scalar and pseudoscalar densities or combination of vector and axial vector currents so that the zero mode contributions are suppressed in  $Z_\Gamma$ . We can do the latter because the overlap fermion respects chiral symmetry on the lattice.

For scalar and pseudoscalar, we can use Eq. (4) to rewrite Eq. (1) as

$$Z_S Z_q \Lambda_I(p^2 = \mu^2) = I \tag{21}$$

and

$$Z_P Z_q \Lambda_{\gamma_5}(p^2 = \mu^2) = \gamma_5. \tag{22}$$

If  $Z_{SP} \equiv Z_S = Z_P$ , then we have

$$Z_{SP} Z_q (\Lambda_I \pm \Lambda_{\gamma_5}) = I \pm \gamma_5, \tag{23}$$

and thus

$$Z_{SP} Z_q \frac{1}{12} \text{Tr}(\Lambda_I \pm \Lambda_{\gamma_5}) = 1. \tag{24}$$

Eq. (6) and Eq. (9) give us

$$\Lambda_I \pm \Lambda_{\gamma_5} = S^{-1}(p) \left[ \frac{1}{N} \sum_{i=1}^N S_i(p|0)(I \pm \gamma_5)\gamma_5 S_i^\dagger(p|0)\gamma_5 \right] S^{-1}(p). \tag{25}$$

For zero modes with positive chirality,  $S_i(p|0)(I - \gamma_5) = 0$ , while for zero modes with negative chirality,  $S_i(p|0)(I + \gamma_5) = 0$ . Therefore, the zero mode contribution in the Green function combination  $G_S(p) \pm G_P(p)$  are removed. We can use Eq. (24) to obtain a  $Z_{SP}$  which has a suppressed zero mode contribution (Note that  $S^{-1}(p)$  still contains zero modes).

Similarly, for vector and axial vector currents, Eq. (1) gives

$$Z_V Z_q \Lambda_{\gamma_\mu}(p^2 = \mu^2) = \gamma_\mu, \tag{26}$$

and

$$Z_A Z_q \Lambda_{\gamma_\mu \gamma_5}(p^2 = \mu^2) = \gamma_\mu \gamma_5. \tag{27}$$

Letting  $Z_{VA} \equiv Z_V = Z_A$ , we obtain

$$\gamma_\mu Z_{VA} Z_q (\Lambda_{\gamma_\mu} \pm \Lambda_{\gamma_\mu \gamma_5}) = I \pm \gamma_5 \tag{28}$$

and subsequently (after the index  $\mu$  is averaged)

$$Z_{VA} Z_q \frac{1}{48} \text{Tr}[(\Lambda_{\gamma_\mu} \pm \Lambda_{\gamma_\mu \gamma_5})\gamma_\mu] = 1. \tag{29}$$

Similar to Eq. (25), we have

$$\Lambda_{\gamma_\mu} \pm \Lambda_{\gamma_\mu \gamma_5} = S^{-1}(p) \left[ \frac{1}{N} \sum_{i=1}^N S_i(p|0)\gamma_\mu(I \pm \gamma_5)\gamma_5 S_i^\dagger(p|0)\gamma_5 \right] S^{-1}(p). \tag{30}$$

For zero modes with positive chirality,  $S_i(p|0)\gamma_\mu(I + \gamma_5) = S_i(p|0)(I - \gamma_5)\gamma_\mu = 0$ . For those with negative chirality,  $S_i(p|0)\gamma_\mu(I - \gamma_5) = S_i(p|0)(I + \gamma_5)\gamma_\mu = 0$ . Therefore,  $Z_{VA}$  calculated from Eq. (29) has a suppressed zero mode contribution.

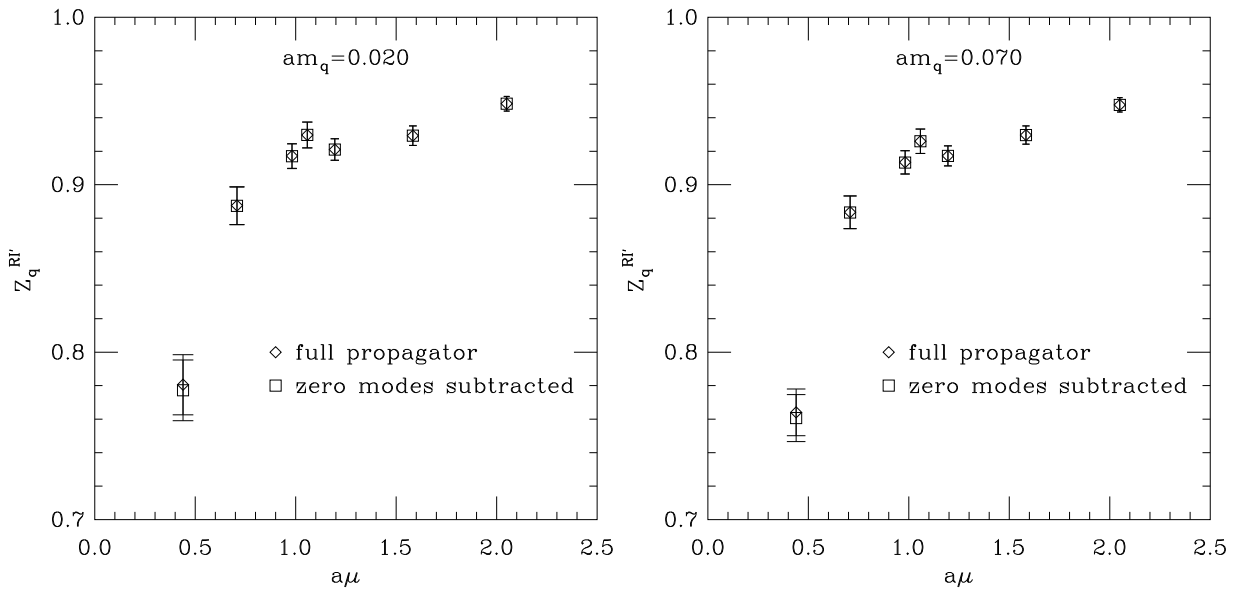


FIG. 1:  $Z_q^{RI'}$  vs.  $a\mu$  for bare quark mass  $am_q = 0.020$  and  $0.070$ .  $Z_q^{RI'}$  obtained from the full propagator (diamond) is compared with that obtained from the propagator with zero mode contribution subtracted (square).

### III. NUMERICAL RESULTS

The data set that we use contains 40 gauge configurations in the quenched approximation with the Wilson gauge action. The lattice size is  $16^4$  and the gauge coupling  $\beta = 6.1$ . The bare quark masses in lattice units are  $am_q = 0.015, 0.020, 0.025, 0.035, 0.050$  and  $0.070$ . The lattice spacing  $a$  is (a): 0.08 fm determined from the interpolation formula of Ref. [17] using the Sommer parameter or (b): 0.09 fm from the measured rho mass. Therefore,  $a\mu = 0.811$  or  $a\mu = 0.913$  corresponds to  $\mu = 2$  GeV accordingly. In the following analysis, the statistical errors are obtained by a Jackknife average with one configuration removed each time.

#### A. $Z_q^{RI'}$ and $Z_m^{RI'}$

The quark field renormalization constant  $Z_q^{RI'}$  is calculated with Eq. (7). The results for two examples of bare quark masses are shown in Fig. 1. The comparison between  $Z_q^{RI'}$  obtained from the full propagator and the propagator with zero mode subtracted is also shown in the same graph. There is no difference within error bars.

The full lattice quark propagator takes the form

$$S(p) = \frac{Z(p)}{i\gamma \cdot q(p) + M(p)}. \quad (31)$$

Here  $q(p)$  is the kinematic momentum depending on the lattice quark action one uses. At large momentum  $p$ , because of asymptotic freedom the propagator should go back to the free quark propagator. i.e.  $Z(p) \rightarrow 1$  and  $M(p)$  goes to the bare quark mass. Fig. 2 shows  $(1/12)\text{Tr}(S^{-1}(p))$  versus  $ap$  for two examples of bare quark masses with  $S(p)$  determined from Eq. (10). Results from the full propagator and from the propagator with zero mode contribution subtracted are compared in the graph. As is expected,  $(1/12)\text{Tr}(S^{-1}(p))$  approaches the bare quark mass at large momentum. Apparently, only at small momentum and small quark mass does the zero mode contribution make a difference.

If we define a renormalized quark mass  $m(\mu)$  by

$$m(\mu) = Z_m(\mu)m_0, \quad (32)$$

where  $m_0$  is the bare quark mass, then  $Z_m(\mu)$  is fixed in the RI' scheme by

$$(Z_m^{RI'})^{-1} = \lim_{m \rightarrow 0} \frac{12m_0}{Z_q^{RI'} \text{Tr}(S^{-1}(p))} \Big|_{p^2=\mu^2}. \quad (33)$$

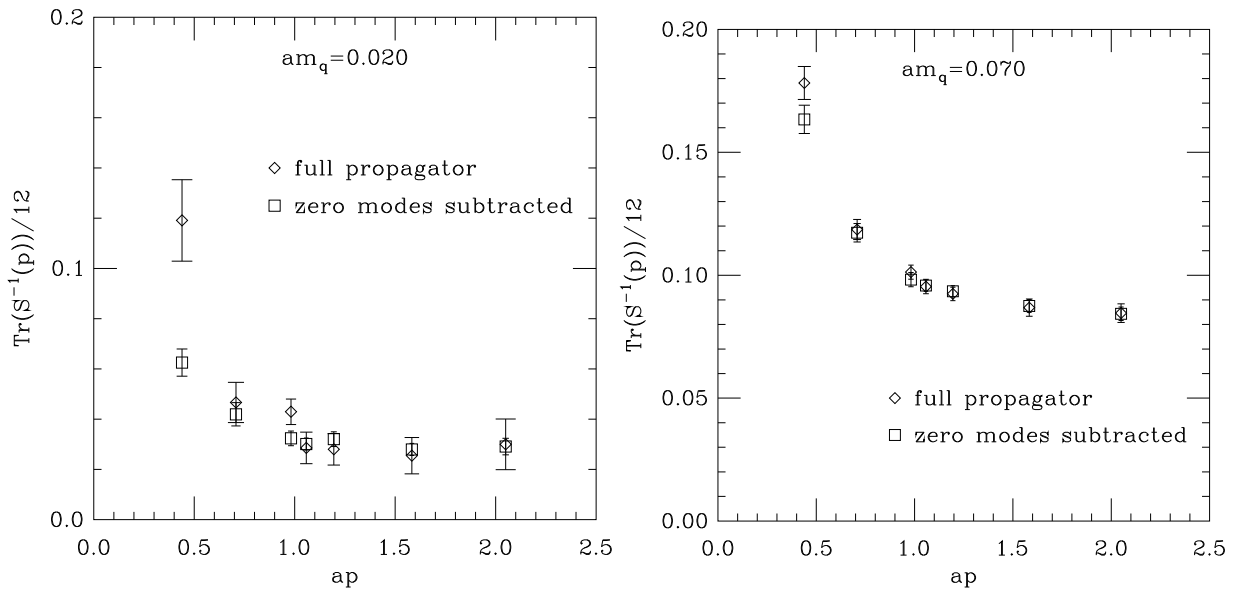


FIG. 2:  $(1/12)\text{Tr}(S^{-1}(p))$  vs.  $ap$  for bare quark masses  $am_q = 0.020$  and  $0.070$ . Results from the full propagator (diamond) and from the propagator with zero mode contribution subtracted (square) are compared. Zero mode contribution is important only at small momentum and small quark mass.

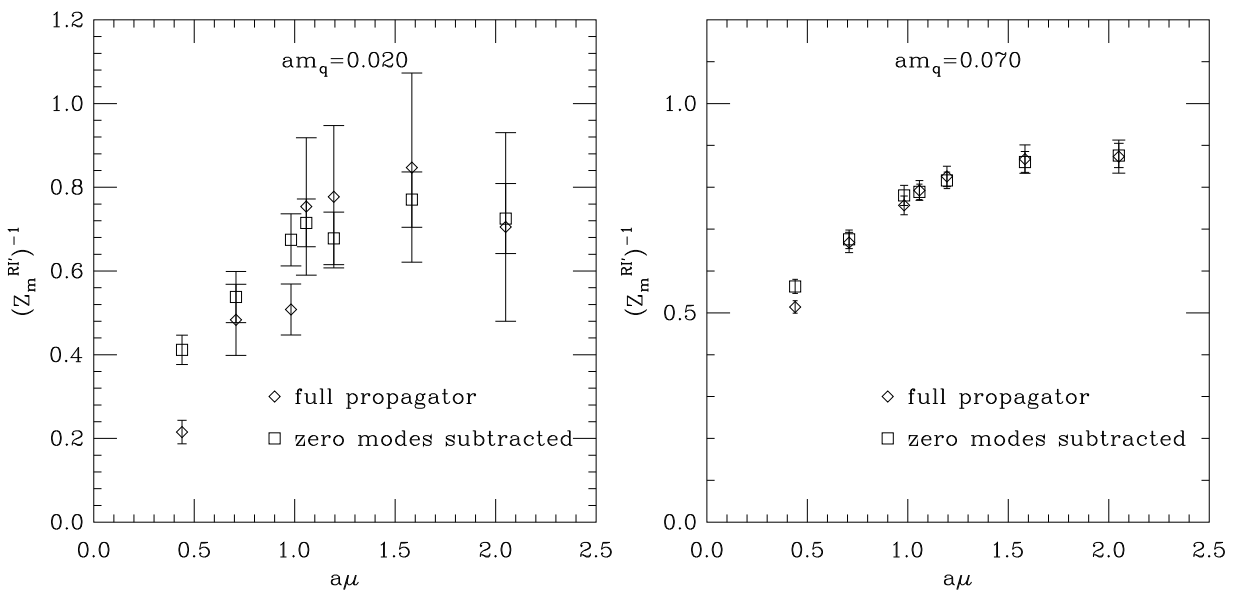


FIG. 3:  $(Z_m^{RI'})^{-1}$  for bare quark masses  $am_q = 0.020$  and  $0.070$ . Diamonds are from the full propagator and squares from the propagator with zero mode contribution subtracted.

At finite quark masses, the renormalization conditions of RI' scheme are compatible with the Ward identities [3, 18] at large  $\mu^2$ , therefore we expect  $Z_m^{RI'} = Z_S^{-1}$  at large  $\mu^2$ . The numerical results of  $(Z_m^{RI'})^{-1}$  are shown in Fig. 3. The error bar at small quark mass is large. A zero mode contribution is visible only at low momentum. We will compare  $(Z_m^{RI'})^{-1}$  with  $Z_S$  later.

### B. $Z_S^{RI'}$ and $Z_P^{RI'}$

The results for  $Z_S$  and  $Z_P$  are shown in Fig. 4. At low quark mass and momentum region, the zero mode subtracted propagators give different values of  $Z_S$  and  $Z_P$  (we will label them as  $Z_S^{NZ}$  and  $Z_P^{NZ}$  in the following) from those

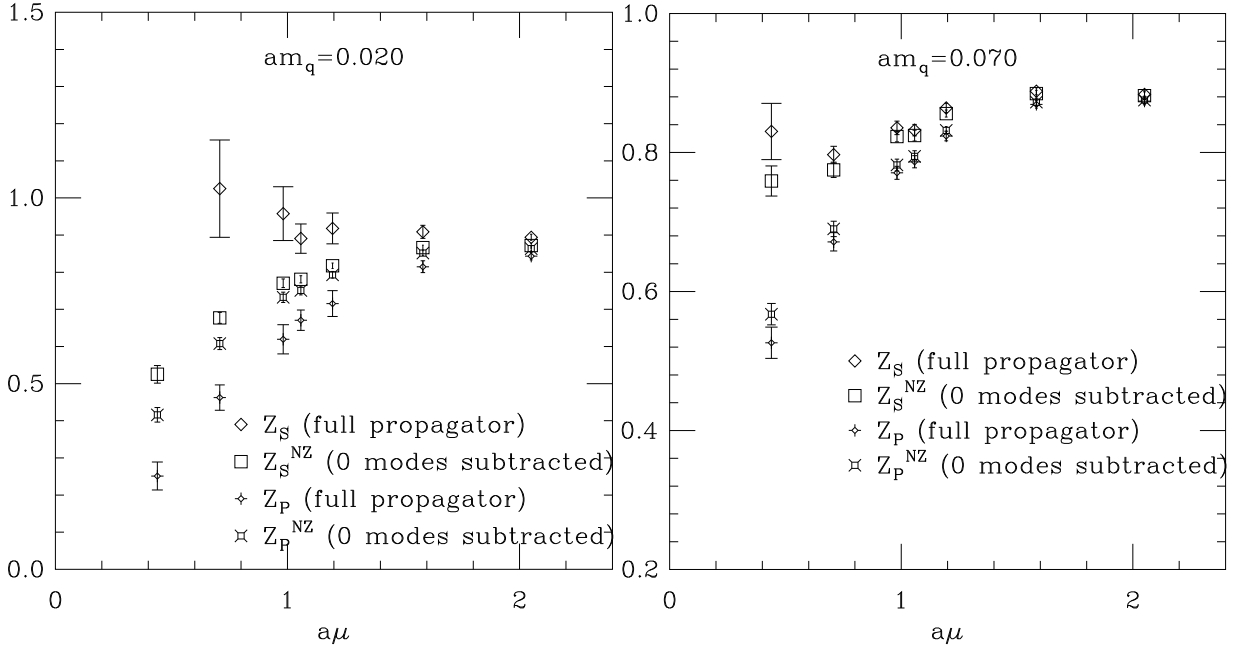


FIG. 4:  $Z_S$  and  $Z_P$  from the full propagators and the zero modes subtracted (labeled as  $Z_S^{NZ}$  and  $Z_P^{NZ}$ ) propagators. The left is for quark mass  $am_q = 0.020$ , the right  $am_q = 0.070$ .

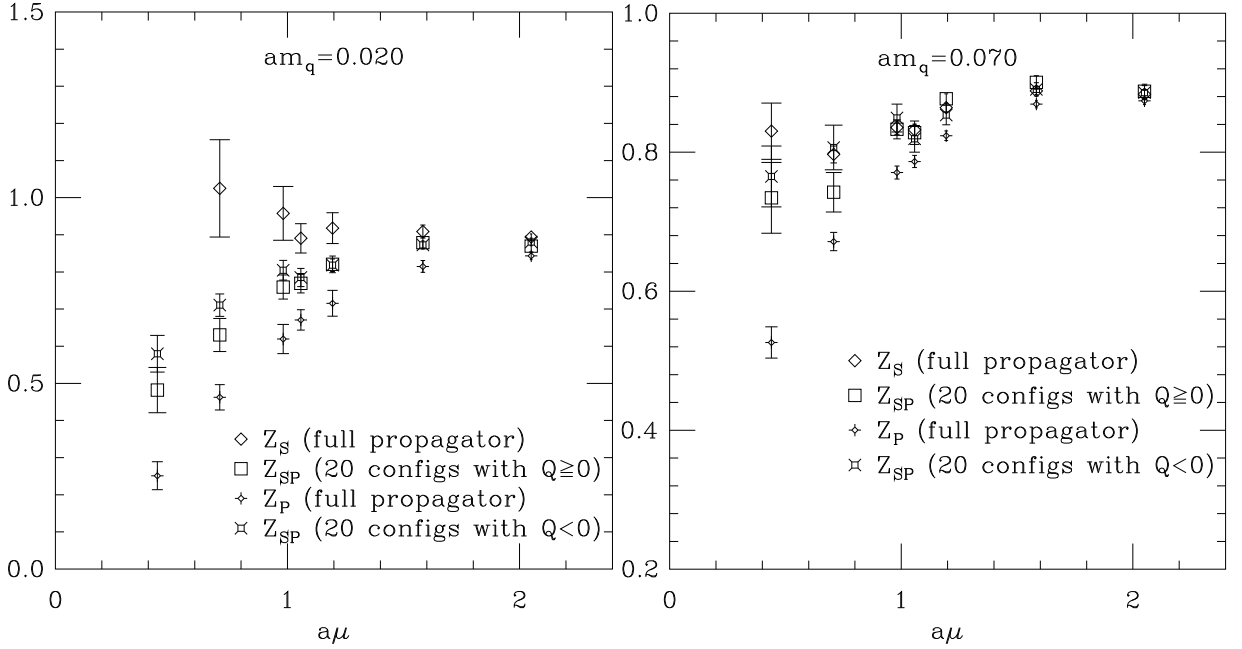


FIG. 5:  $Z_{SP}$  obtained by using Eq. (24) comparing with  $Z_S$  and  $Z_P$ . The left is for quark mass  $am_q = 0.020$ , the right  $am_q = 0.070$ .  $Q$  is the topological charge.

obtained with the full propagators. The pseudoscalar density couples to the Goldstone boson channel but the coupling is suppressed at large  $\mu$  [3]. Therefore we see a difference between  $Z_S$  and  $Z_P$  at small  $\mu$ , but no difference at large  $\mu$ .

As was discussed in Section II, we can also use Eq. (24) to suppress the zero modes and obtain  $Z_{SP}$ . Fig. 5 shows the results of  $Z_{SP}$  comparing with  $Z_S$  and  $Z_P$ . The  $Z_{SP}$ 's from configurations with topological charge  $Q \geq 0$  and  $Q < 0$  are quite close to each other. At small quark mass and small  $\mu$ ,  $Z_{SP}$  is apparently different from  $Z_S$  and  $Z_P$  as can be seen in the graph for  $am_q = 0.020$  in Fig. 5.  $Z_{SP}$  agrees with  $Z_S^{NZ}$  and  $Z_P^{NZ}$  obtained from the zero mode

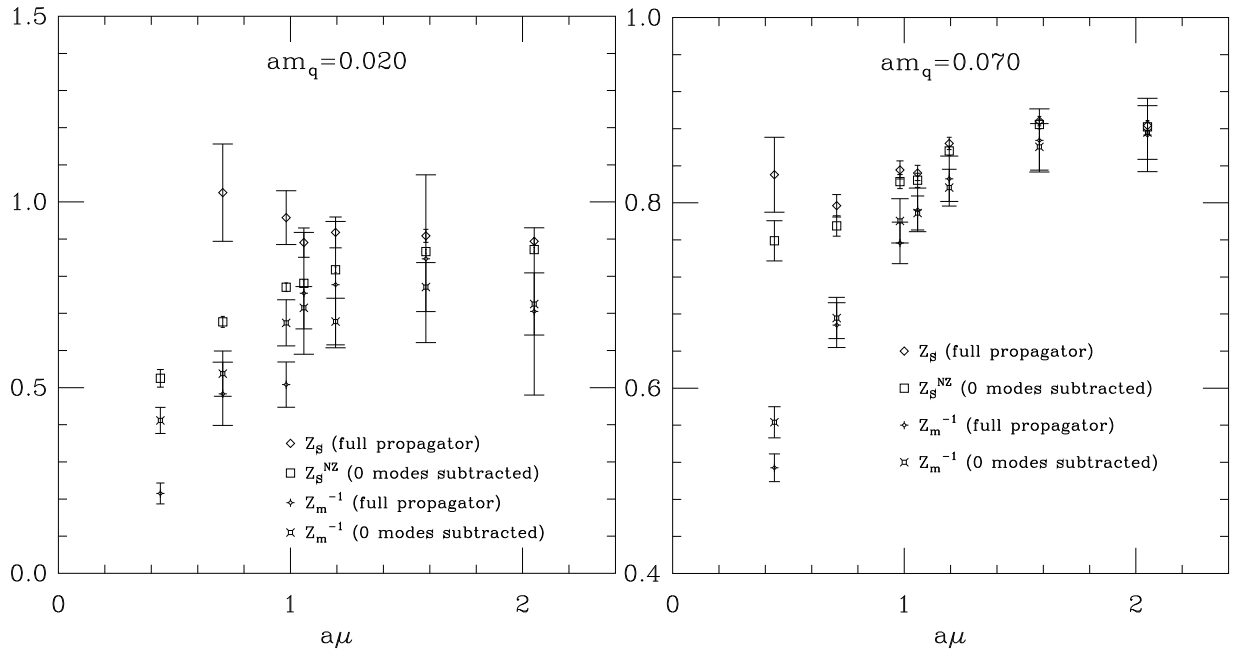


FIG. 6:  $(Z_m^{RI'})^{-1}$  compared with  $Z_S^{RI'}$ . At large  $\mu$ ,  $(Z_m^{RI'})^{-1} = Z_S^{RI'}$  is well satisfied.

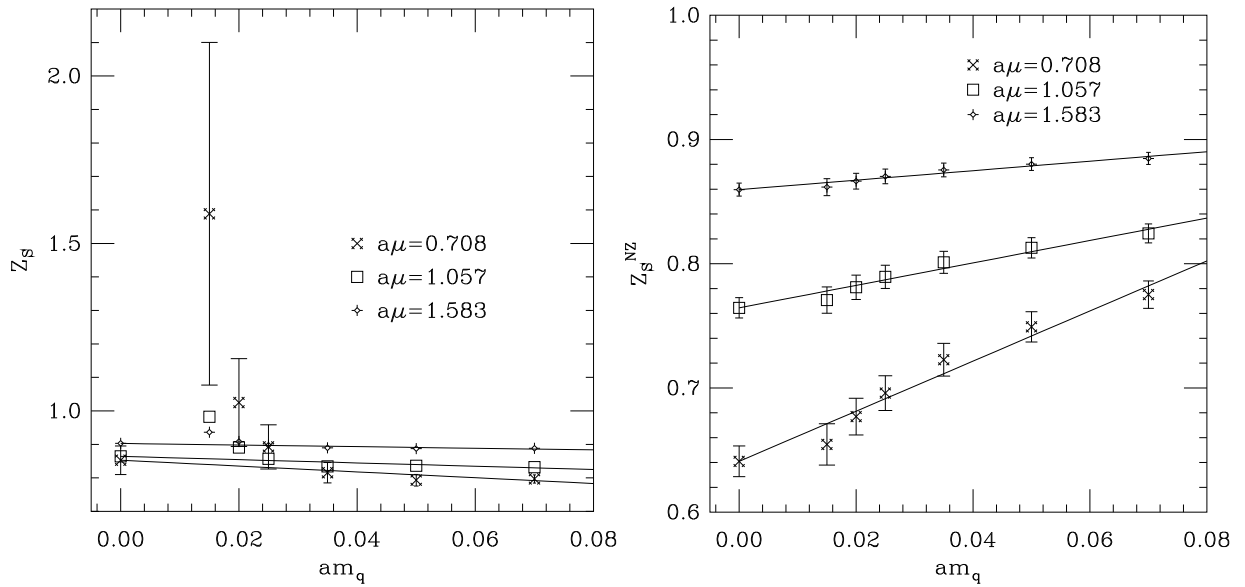


FIG. 7: Linear extrapolation of  $Z_S$  to the chiral limit. The left is for  $Z_S$  obtained from full propagators. The data do not support a linear extrapolation. We did it anyway just for comparison. The right is for  $Z_S$  obtained from zero mode subtracted propagators (labeled as  $Z_S^{NZ}$ ). At small quark mass,  $Z_S$  and  $Z_S^{NZ}$  are very different.

subtracted propagators in Fig. 4 for  $am_q = 0.020$ . For large quark mass, for example  $am_q = 0.070$ , and small  $\mu$ ,  $Z_{SP}$  is close to  $Z_S$  but very different from  $Z_P$ .  $Z_{SP}$  from Eq. (24) is still contaminated by the coupling to the Goldstone boson. Thus, this means that suppressing the zero modes can suppress the coupling to the Goldstone boson. We do not see this behavior in Fig. 4 for  $am_q = 0.070$ . The  $Z_P^{NZ}$  from the zero mode subtracted propagator is very close to the  $Z_P$  from the full propagator. However, we should notice that subtracting zero modes directly from the propagators amounts to a modification of the quenched theory. To further investigate the zero modes, a quenched artifact, simulations with dynamical fermions are necessary.

The comparison of  $(Z_m^{RI'})^{-1}$  with  $Z_S^{RI'}$  is given in Fig. 6. We see a good agreement between  $(Z_m^{RI'})^{-1}$  and  $Z_S^{RI'}$  at large  $\mu$  as expected.



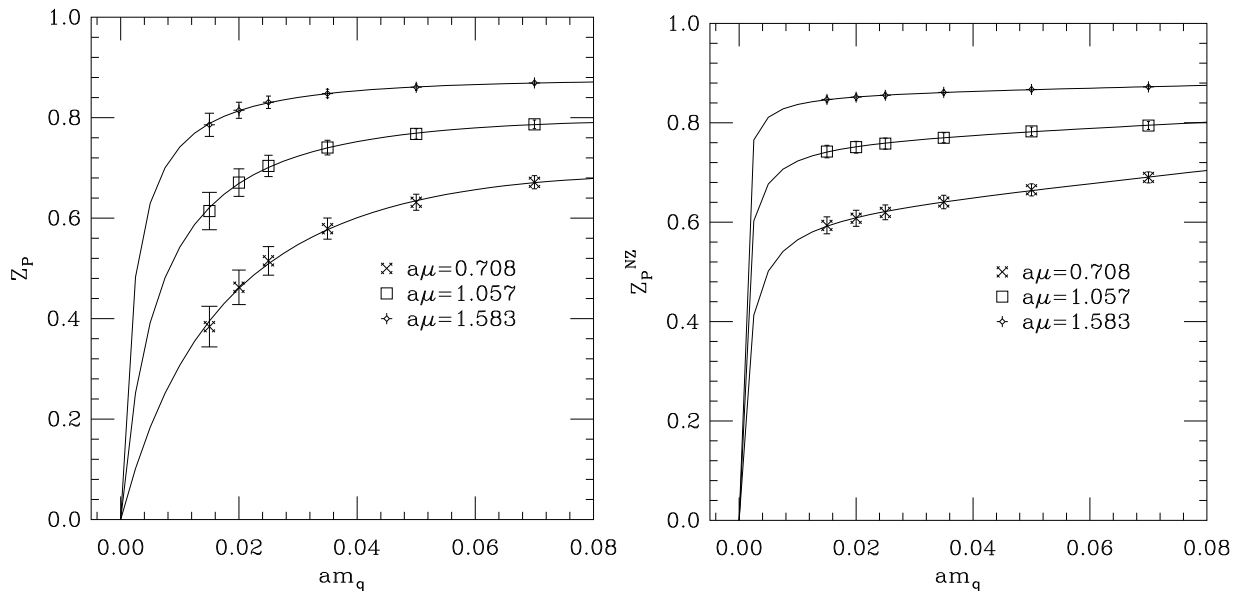


FIG. 8: Extrapolation of  $Z_P$  to the chiral limit using Eq. (34).  $Z_P$  in the left graph is obtained by using the full propagator, while  $Z_P^{NZ}$  in the right graph is obtained by using the propagator with zero modes subtracted. Both are fits after the last configuration is dropped during the Jackknife average process.

In Fig. 7, 8 and 9,  $Z_S$ ,  $Z_S^{NZ}$ ,  $Z_P$ ,  $Z_P^{NZ}$  and  $Z_{SP}$  (average from configurations with  $Q \geq 0$  and  $Q < 0$ ) are plotted versus the quark mass at  $a\mu = 0.708$ , 1.057 and 1.583 along with the extrapolation to the chiral limit. A linear fit is used for  $Z_S$  and  $Z_S^{NZ}$ . The data for  $Z_S$  which is obtained from the full propagator do not support a linear extrapolation as is shown in Fig. 7. For  $Z_P$ , we see similar behavior as was seen in [5, 6, 19, 20, 21] since the pseudoscalar density couples to the Goldstone boson channel. As in [6, 21], we use

$$\frac{1}{Z_P(\mu^2, m)} = \frac{A(\mu^2)}{am_q} + B(\mu^2) + C(\mu^2)(am_q) \quad (34)$$

to fit  $Z_P$  and then remove the pole term  $A(\mu^2)/am_q$  to obtain  $Z_P^{NP} \equiv B(\mu^2)^{-1}$  in the chiral limit. The fit is good as can be seen in Fig. 8. Fig. 8 shows one example of the fit when we drop one configuration and obtain  $Z_P$  with the rest configurations during the Jackknife average process.

We also use Eq. (34) to extrapolate  $Z_{SP}$  to the chiral limit to obtain  $Z_{SP}^{NP} \equiv B(\mu^2)^{-1}$ . The fit is shown in Fig. 9.

Values of  $Z_S$ ,  $Z_P^{NP}$ ,  $Z_S^{NZ}$ ,  $(Z_P^{NZ})^{NP}$  and  $Z_{SP}^{NP}$  in the RI' scheme in the chiral limit are listed in Table I. In the table, the superscripts (a) and (b) indicate the two different ways of determining the lattice spacing. We could not get  $Z_S$  for the smallest momentum because the signal is noisy in our data.  $Z_S$  and  $Z_P^{NP}$  are different from each other at small  $\mu$  so that the  $\overline{MS}$  values of them differ from each other. The  $\overline{MS}$  values are obtained by using the conversion formulas in Section IV and a linear interpolation from the two closest  $\mu$  value of the data. After subtracting the zero modes from the quark propagators, we get  $Z_S^{NZ}$  and  $(Z_P^{NZ})^{NP}$ . They are in good agreement with each other, which is expected from chiral symmetry, but are very different from  $Z_S$  and  $Z_P^{NP}$ . The other way of suppressing the zero modes gives us  $Z_{SP}^{NP}$ . Since the zero mode effects are much more apparent in  $Z_S$  and  $Z_P$ , we will use  $Z_S^{NZ}$ ,  $(Z_P^{NZ})^{NP}$  and  $Z_{SP}^{NP}$  to compare with perturbative calculations.

### C. $Z_V^{RI'}$ and $Z_A^{RI'}$

In Fig. 10, the renormalization constants of the vector current  $Z_V$  and axial vector current  $Z_A$  are given. For clarity, at each value of the momentum  $a\mu$ , the x-positions of  $Z_V$  and  $Z_A$  are shifted a little in the graph. As is shown in the graph,  $Z_V$  and  $Z_A$  are independent of the scale at large  $\mu$  ( $a\mu > 0.7$ ), and  $Z_V = Z_A$  within statistical errors. At low  $\mu$ ,  $Z_A$  is bigger than  $Z_V$ . We think it is because the axial vector current is coupled to the Goldstone boson.  $Z_V^{NZ}$  and  $Z_A^{NZ}$  obtained from quark propagators with zero modes subtracted are compared with  $Z_V$  and  $Z_A$  in Fig. 11. Apparently, zero modes have little effect on  $Z_V$  and  $Z_A$ .  $Z_{VA}$  obtained from Eq. (29) is shown in Fig. 12. It agrees with the average of  $Z_V$  and  $Z_A$ . This confirms that zero mode contribution doesn't matter in the computation of  $Z_V$  and  $Z_A$ .

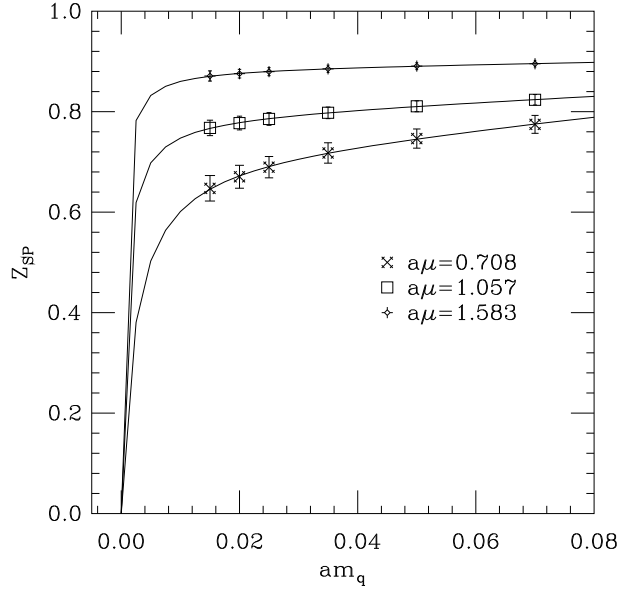


FIG. 9: Extrapolation of  $Z_{SP}$  to the chiral limit using Eq. (34).  $Z_{SP}$  is the average from configurations with  $Q \geq 0$  and  $Q < 0$ .

$a\mu$	$\mu^{(a)}$ (GeV)	$\mu^{(b)}$ (GeV)	$Z_S$	$Z_P^{NP}$	$Z_S^{NZ}$	$(Z_P^{NZ})^{NP}$	$Z_{SP}^{NP}$
0.439	1.08	0.96		1.31(6)	0.43(2)	0.455(2)	0.642(2)
0.708	1.75	1.55	0.85(4)	0.97(1)	0.64(1)	0.631(1)	0.732(2)
0.982	2.42	2.15	0.89(3)	0.94(2)	0.753(9)	0.755(1)	0.828(2)
1.057	2.61	2.32	0.86(2)	0.887(9)	0.764(8)	0.7685(9)	0.7972(9)
1.194	2.95	2.62	0.89(2)	0.92(1)	0.805(5)	0.817(1)	0.8489(9)
1.583	3.91	3.47	0.90(1)	0.906(4)	0.860(5)	0.8611(3)	0.8874(6)
2.050	5.06	4.49	0.896(7)	0.901(2)	0.868(6)	0.8725(2)	0.8826(4)
$\overline{MS}^{(a)}$	2 GeV		1.01(2)	1.12(1)	0.79(5)	0.79(5)	0.89(4)
$\overline{MS}^{(b)}$		2 GeV	1.01(1)	1.091(9)	0.83(3)	0.83(4)	0.93(3)

TABLE I: Values of  $Z_S$ ,  $Z_P^{NP}$ ,  $Z_S^{NZ}$ ,  $(Z_P^{NZ})^{NP}$  and  $Z_{SP}^{NP}$  in the RI' scheme in the chiral limit. The  $\overline{MS}(2 \text{ GeV})$  value is obtained from a linear interpolation from the two closest  $\mu$  values of the data. The lattice spacing is (a): 0.08 fm from Sommer parameter or (b): 0.09 fm from the measured rho mass. Correspondingly, we get two  $\overline{MS}(2 \text{ GeV})$  values.  $Z_S$  and  $Z_P^{NP}$  contains zero modes and seen to be quite different from the  $Z$ 's which contains no zero modes.

The RI' scheme values of  $Z_V$ ,  $Z_A$ ,  $Z_V^{NZ}$  and  $Z_A^{NZ}$  in the chiral limit are given in Table II. The superscripts (a) and (b) in the table indicate the two different ways of determining the lattice spacing. The  $\overline{MS}$  values are obtained by using the conversion formulas in Section IV.  $Z_V = Z_A$  is very well satisfied as expected since the overlap fermion respects chiral symmetry on the lattice. The linear extrapolation to the chiral limit is shown in Fig. 13.

#### IV. CONVERSION TO $\overline{MS}$

The ratio  $Z_{\Gamma}^{\overline{MS}}(\mu^2)/Z_{\Gamma}^{RI'}(\mu^2)$  connects the  $\overline{MS}$  scheme to the RI' scheme is computed by continuum perturbation theory. There is a need to determine the coupling constant  $\alpha_s(\mu)$  in the ratio. We obtain  $\alpha_s^{\overline{MS}}(\mu)$  by first measuring the trace of the plaquette operator  $U_{plaq}$  (the  $1 \times 1$  Wilson loop), which can give us  $\alpha_s^V(3.41/a)$  [9]. Then  $a\Lambda_V$  and  $a\Lambda_{\overline{MS}}$  are calculated. Finally  $\alpha_s^{\overline{MS}}(\mu)$  is determined by

$$(\alpha_s^{\overline{MS}}(\mu))^{-1} = \beta_0 \ln(\mu/\Lambda_{\overline{MS}})^2 + (\beta_1/\beta_0) \ln \ln(\mu/\Lambda_{\overline{MS}})^2, \quad (35)$$

where  $\beta_0 = 11/4\pi$  and  $\beta_1 = 102/16\pi^2$  for the quenched approximation. If the lattice spacing  $a = 0.08$  fm from the Sommer parameter, we find  $\alpha_s^{\overline{MS}}(\mu = 2 \text{ GeV}) = \alpha_s^{\overline{MS}}(0.811/a) = 0.2038$ . If  $a = 0.09$  fm from the measured rho mass, then  $\alpha_s^{\overline{MS}}(\mu = 2 \text{ GeV}) = \alpha_s^{\overline{MS}}(0.913/a) = 0.1940$ .

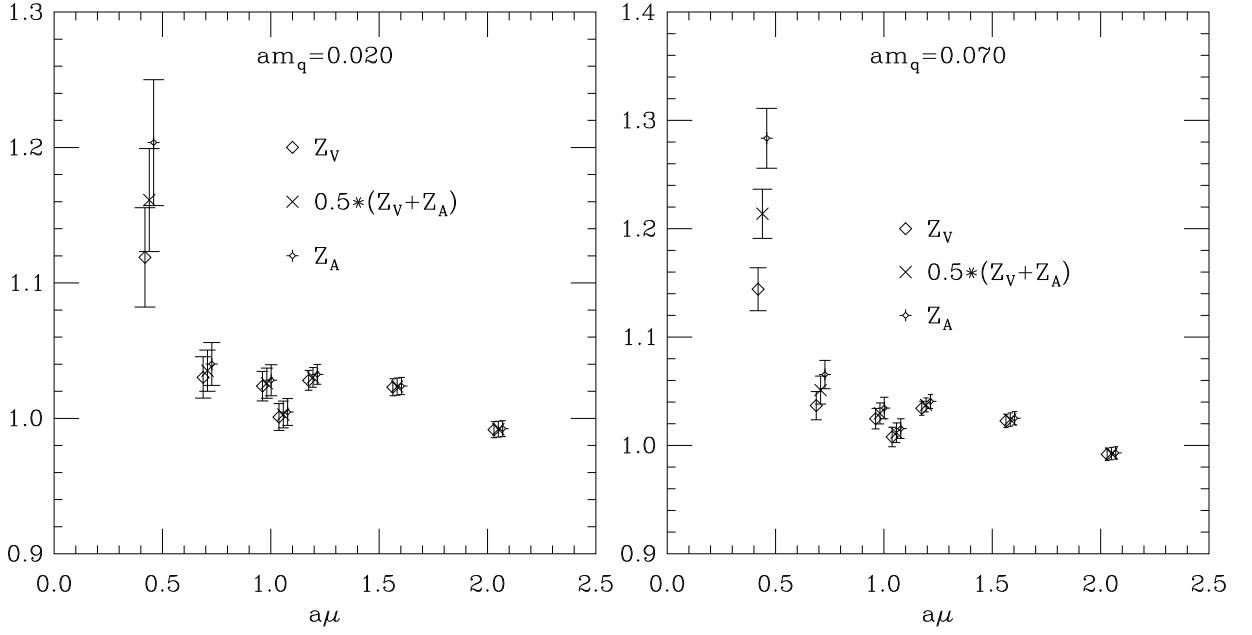


FIG. 10:  $Z_V, Z_A$  and their average versus  $a\mu$  for quark masses  $am_q = 0.020$  and  $0.070$ . For clarity, at each value of the momentum  $a\mu$ , the x-positions of  $Z_V$  and  $Z_A$  are shifted a little.

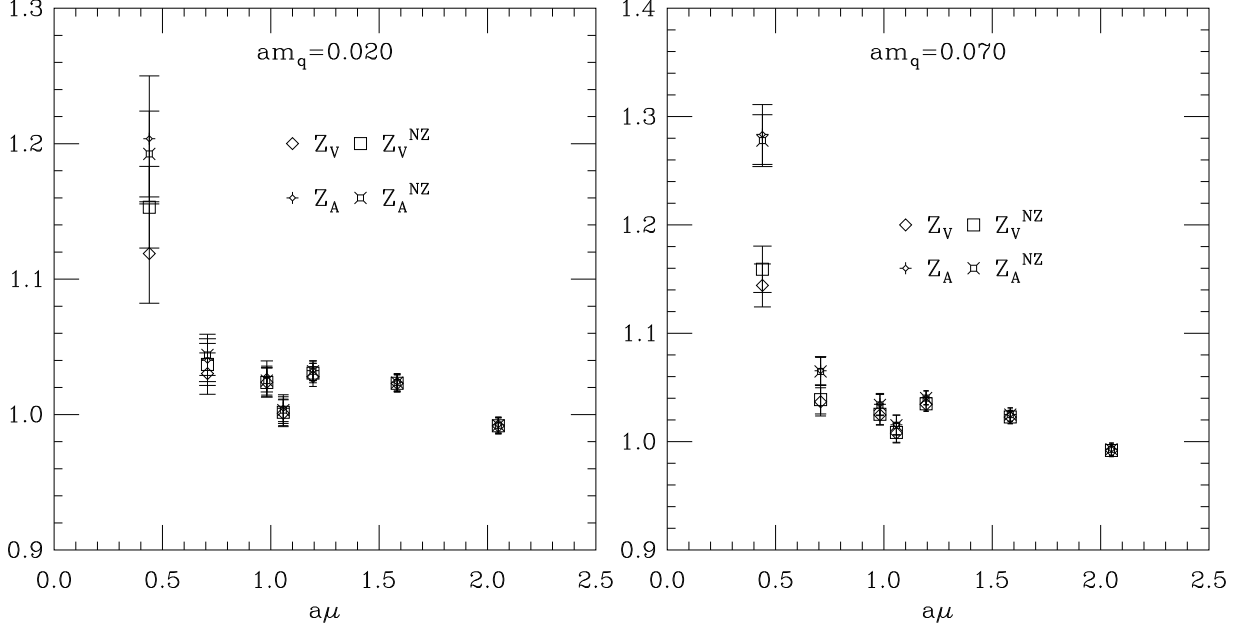


FIG. 11:  $Z_V^{NZ}$  and  $Z_A^{NZ}$  compared with  $Z_V$  and  $Z_A$  for quark masses  $am_q = 0.020$  and  $0.070$ .

For the scalar and pseudoscalar, in the Landau gauge and 3-loop order, the conversion ratio is [18, 22]

$$\begin{aligned} \frac{Z_S^{\overline{MS}}}{Z_S^{RI'}} = \frac{Z_P^{\overline{MS}}}{Z_P^{RI'}} = & 1 + \frac{16}{3} \frac{\alpha_s}{4\pi} + \left( \frac{4291}{18} - \frac{152\zeta_3}{3} \right) \left( \frac{\alpha_s}{4\pi} \right)^2 \\ & + \left( \frac{3890527}{324} - \frac{224993\zeta_3}{54} + \frac{2960\zeta_5}{9} \right) \left( \frac{\alpha_s}{4\pi} \right)^3 + O(\alpha_s^4), \end{aligned} \quad (36)$$

where  $\zeta_n$  is the Riemann zeta function evaluated at  $n$ . Substituting  $\alpha_s^{\overline{MS}}(\mu = 2 \text{ GeV}) = 0.2038$  or  $0.1940$  into the above equation, we get  $Z_S^{\overline{MS}}/Z_S^{RI'} = Z_P^{\overline{MS}}/Z_P^{RI'} = 1 + 0.08650 + 0.04668 + 0.03131 = 1.1645$  or  $1 + 0.08234 + 0.04230 +$

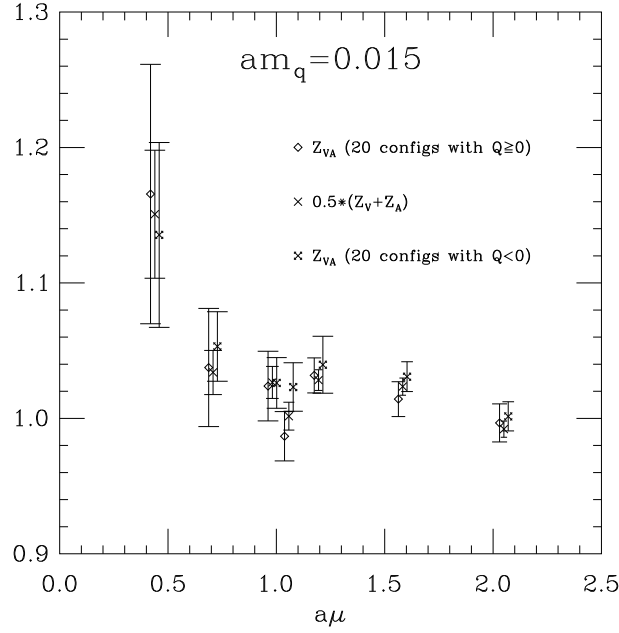


FIG. 12:  $Z_{VA}$  and  $0.5(Z_V + Z_A)$  at the smallest quark mass  $am_q = 0.015$ .

$a\mu$	$\mu^{(a)}$ (GeV)	$\mu^{(b)}$ (GeV)	$Z_V$	$Z_A$	$Z_V^{NZ}$	$Z_A^{NZ}$
0.439	1.08	0.96	1.11(3)	1.17(4)	1.15(2)	1.16(3)
0.708	1.75	1.55	1.03(1)	1.03(1)	1.04(1)	1.04(1)
0.982	2.42	2.15	1.024(9)	1.026(10)	1.023(9)	1.022(9)
1.057	2.61	2.32	0.998(9)	1.000(9)	0.999(8)	0.999(8)
1.194	2.95	2.62	1.026(6)	1.029(6)	1.029(6)	1.029(6)
1.583	3.91	3.47	1.023(5)	1.023(6)	1.023(6)	1.023(6)
2.050	5.06	4.49	0.992(5)	0.992(5)	0.992(5)	0.992(5)
$\overline{MS}^{(a)}$	2 GeV		1.022(2)	1.023(1)	1.028(6)	1.028(7)
$\overline{MS}^{(b)}$		2 GeV	1.021(1)	1.022(1)	1.022(4)	1.022(4)

TABLE II: Values of  $Z_V$ ,  $Z_A$ ,  $Z_V^{NZ}$  and  $Z_A^{NZ}$  in the RI' scheme in the chiral limit. The  $\overline{MS}(2 \text{ GeV})$  value is obtained from a linear interpolation from the two closest  $\mu$  values of the data. The lattice spacing is (a): 0.08 fm from Sommer parameter or (b): 0.09 fm from the measured rho mass. Correspondingly, we get two  $\overline{MS}(2 \text{ GeV})$  values.

0.02701 = 1.1516.

For the vector and axial vector, since  $Z_V^{RI} = Z_V^{\overline{MS}}$  and the difference between RI scheme and RI' scheme is only the different definition of the quark field renormalization constants, we have

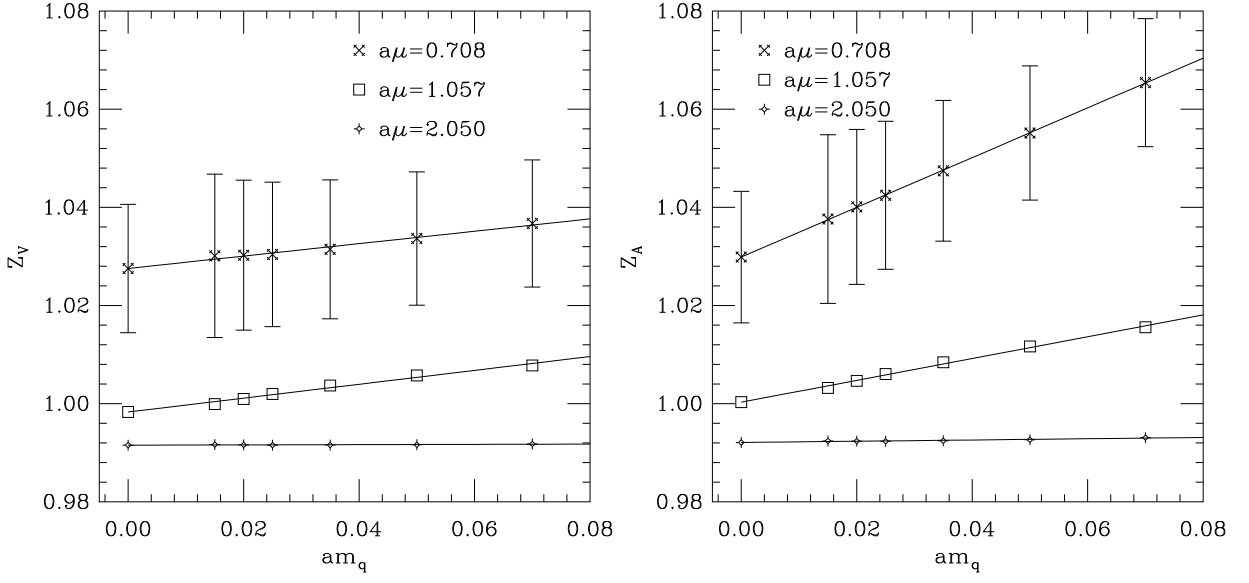
$$\frac{Z_A^{\overline{MS}}}{Z_A^{RI'}} = \frac{Z_V^{\overline{MS}}}{Z_V^{RI'}} = \frac{Z_V^{RI}}{Z_V^{RI'}} = \frac{Z_q^{RI'}}{Z_q^{RI}} = \frac{Z_q^{RI'}/Z_q^{\overline{MS}}}{Z_q^{RI}/Z_q^{\overline{MS}}} \quad (37)$$

$Z_q^{RI'}/Z_q^{\overline{MS}}$  and  $Z_q^{RI}/Z_q^{\overline{MS}}$  were calculated in Ref. [18, 22] to 3-loop, so we find

$$\frac{Z_A^{\overline{MS}}}{Z_A^{RI'}} = \frac{Z_V^{\overline{MS}}}{Z_V^{RI'}} = 1 - \frac{67}{6} \left( \frac{\alpha_s}{4\pi} \right)^2 - \left( \frac{52321}{72} - \frac{607\zeta_3}{4} \right) \left( \frac{\alpha_s}{4\pi} \right)^3 + O(\alpha_s^4) \quad (38)$$

The numerical value at  $\mu = 2 \text{ GeV}$  is  $(1 + 0 - 0.00294 - 0.00232) = 0.9947$  or  $(1 + 0 - 0.00266 - 0.00200) = 0.9953$ .

In Table I and II, the  $\overline{MS}$  values at  $\mu = 2 \text{ GeV}$  are obtained from linear interpolations between the two closest  $\mu$  values of the data.

FIG. 13: Extrapolation of  $Z_V$  and  $Z_A$  to the chiral limit.

$Z_{S,P}$	$\alpha_s^V(1.96/a)$	$\alpha_s^V(1.52/a)$	$\alpha_s^{\overline{MS}}(1.96/a)$	$\alpha_s^{\overline{MS}}(1.52/a)$
	1.010	1.011	1.008	1.009
$Z_{V,A}$	$\alpha_s^V(1.26/a)$	$\alpha_s^V(1.46/a)$	$\alpha_s^{\overline{MS}}(1.26/a)$	$\alpha_s^{\overline{MS}}(1.46/a)$
	0.989	0.990	0.991	0.992

TABLE III: Values of  $Z_{S,P}$  and  $Z_{V,A}$  at  $a\mu = 1$  for HYP-planar overlap action from perturbative calculation in Ref. [10].

## V. COMPARISON WITH PERTURBATIVE CALCULATIONS

The perturbative calculation in Ref. [10] gives the lattice to  $\overline{MS}$  matching factor  $Z_i = 1 + z_i \alpha_s(q^*)/3\pi$  at  $a\mu = 1$ . Here  $i=S, P, V$  and  $A$  for fermion bilinears. The values of  $z_i$  and the scale  $q^*$  are given in Table V in Ref. [10].

We may use  $\alpha_s^V(q^*)$  run from  $\alpha_s^V(3.41/a)$ , as is determined from the plaquette [9] or  $\alpha_s^{\overline{MS}}(q^*)$  from Eq. (35). The results of  $Z_i$ 's are listed in Table III. The ambiguity in the choice of  $\alpha_s$  and  $q^*$  in perturbation theory is small. We have to run the result of  $Z_{S,P}$  to  $\mu = 2$  GeV to compare with our  $\overline{MS}(2$  GeV) value. We use the two loop formula for the running quark mass given in Ref. [23](Eq. (4.81)). If the inverse lattice spacing is  $1/a = 2.47$  GeV ( $a = 0.08$  fm) from the Sommer parameter, then we find  $Z_{S,P}(2$  GeV) = 0.975 from  $Z_{S,P}(2.47$  GeV) = 1.009. If the inverse lattice spacing is  $1/a = 2.19$  GeV ( $a = 0.09$  fm) from the measured rho mass, then  $Z_{S,P}(2$  GeV) = 0.995. In any case, the value of  $Z_{S,P}$  from perturbative calculation is quite close to 1, while our non-perturbative results 0.79(5)/0.89(4) or 0.83(4)/0.93(3) (see Table I) are not. Thus, perturbative calculation of the matching factors for scalar and pseudoscalar density for HYP-planar overlap action seems unreliable.

Unlike  $Z_S$  or  $Z_P$ ,  $Z_V$  and  $Z_A$  are scale independent. We can compare the values of  $Z_{V,A}$  in Table III directly with our non-perturbative  $\overline{MS}(2$  GeV) results in Table II. All are quite close to one (the shift from one is less than 0.03). This indicates that we can believe in the perturbative calculations of  $Z_V$  and  $Z_A$  for the HYP-planar overlap action.

## VI. SUMMARY AND CONCLUSION

We calculated the renormalization constants of bilinear quark operators non-perturbatively using the HYP-planar overlap action with exact chiral symmetry. By comparing the results with those from perturbative computation, we find that a perturbative calculation is reliable with  $Z_V$  and  $Z_A$ , but not with  $Z_S$  and  $Z_P$ . The exact zero modes of the Dirac operator turn out to be important in calculating  $Z_S$  and  $Z_P$ , while not relevant in calculating  $Z_V$  and  $Z_A$ . After subtracting the zero modes from the quark propagator,  $Z_S = Z_P$  is well satisfied.  $Z_V$  and  $Z_A$  are also in good agreement with each other as is expected from the chiral symmetry of the action. We expect that zero modes will be

much less important in simulations done with dynamical overlap quarks[24].

The perturbative result that actions using HYP-blocked links have matching factors quite close to unity is confirmed for vector and axial vector currents with our HYP-planar overlap action. This does not appear to be the case for the scalar and pseudoscalar densities.

### Acknowledgments

This work was supported by the US Department of Energy.

- 
- [1] H. Neuberger, Phys. Lett. B **417**, 141 (1998) [arXiv:hep-lat/9707022]. H. Neuberger, Phys. Rev. Lett. **81**, 4060 (1998) [arXiv:hep-lat/9806025].
  - [2] A. Hasenfratz and F. Knechtli, Phys. Rev. D **64**, 034504 (2001) [arXiv:hep-lat/0103029]. A. Hasenfratz, R. Hoffmann and F. Knechtli, Nucl. Phys. Proc. Suppl. **106**, 418 (2002) [arXiv:hep-lat/0110168].
  - [3] G. Martinelli, C. Pittori, C. T. Sachrajda, M. Testa and A. Vladikas, Nucl. Phys. B **445**, 81 (1995) [arXiv:hep-lat/9411010].
  - [4] V. Gimenez, L. Giusti, F. Rapuano and M. Talevi, Nucl. Phys. B **531**, 429 (1998) [arXiv:hep-lat/9806006].
  - [5] M. Gockeler *et al.*, Nucl. Phys. B **544**, 699 (1999) [arXiv:hep-lat/9807044].
  - [6] C. Gattringer, M. Gockeler, P. Huber and C. B. Lang, Nucl. Phys. B **694**, 170 (2004) [arXiv:hep-lat/0404006].
  - [7] T. DeGrand [MILC collaboration], Phys. Rev. D **63**, 034503 (2001) [arXiv:hep-lat/0007046].
  - [8] P. H. Ginsparg and K. G. Wilson, Phys. Rev. D **25**, 2649 (1982).
  - [9] G. P. Lepage and P. B. Mackenzie, Nucl. Phys. Proc. Suppl. **20**, 173 (1991). G. P. Lepage and P. B. Mackenzie, Phys. Rev. D **48**, 2250 (1993) [arXiv:hep-lat/9209022].
  - [10] T. DeGrand, Phys. Rev. D **67**, 014507 (2003) [arXiv:hep-lat/0210028].
  - [11] T. DeGrand [MILC Collaboration], Phys. Rev. D **69**, 014504 (2004) [arXiv:hep-lat/0309026].
  - [12] C. W. Bernard and T. DeGrand, Nucl. Phys. Proc. Suppl. **83**, 845 (2000) [arXiv:hep-lat/9909083]. W. j. Lee and S. R. Sharpe, Phys. Rev. D **66**, 114501 (2002) [arXiv:hep-lat/0208018]. W. j. Lee and S. R. Sharpe, Nucl. Phys. Proc. Suppl. **119**, 476 (2003) [arXiv:hep-lat/0208036].
  - [13] M. L. Paciello, S. Petrarca, B. Taglienti and A. Vladikas, Phys. Lett. B **341**, 187 (1994) [arXiv:hep-lat/9409012].
  - [14] L. Giusti, M. L. Paciello, C. Parrinello, S. Petrarca and B. Taglienti, Int. J. Mod. Phys. A **16**, 3487 (2001) [arXiv:hep-lat/0104012].
  - [15] L. Giusti, S. Petrarca, B. Taglienti and N. Tantalo, Phys. Lett. B **541**, 350 (2002) [arXiv:hep-lat/0205009].
  - [16] S. Capitani, M. Gockeler, R. Horsley, P. E. L. Rakow and G. Schierholz, Phys. Lett. B **468**, 150 (1999) [arXiv:hep-lat/9908029].
  - [17] M. Guagnelli, R. Sommer and H. Wittig [ALPHA collaboration], Nucl. Phys. B **535**, 389 (1998) [arXiv:hep-lat/9806005].
  - [18] E. Franco and V. Lubicz, Nucl. Phys. B **531**, 641 (1998) [arXiv:hep-ph/9803491].
  - [19] J. R. Cudell, A. Le Yaouanc and C. Pittori, Phys. Lett. B **454**, 105 (1999) [arXiv:hep-lat/9810058]. J. R. Cudell, A. Le Yaouanc and C. Pittori, Phys. Lett. B **516**, 92 (2001) [arXiv:hep-lat/0101009].
  - [20] L. Giusti and A. Vladikas, Phys. Lett. B **488**, 303 (2000) [arXiv:hep-lat/0005026].
  - [21] D. Becirevic, V. Gimenez, V. Lubicz, G. Martinelli, M. Papinutto and J. Reyes, JHEP **0408**, 022 (2004) [arXiv:hep-lat/0401033].
  - [22] K. G. Chetyrkin and A. Retey, Nucl. Phys. B **583**, 3 (2000) [arXiv:hep-ph/9910332].
  - [23] A. J. Buras, arXiv:hep-ph/9806471.
  - [24] T. DeGrand and S. Schaefer, Phys. Rev. D **71**, 034507 (2005) [arXiv:hep-lat/0412005]; arXiv:hep-lat/0506021.